Original Manuscript

High Performance Polymers

High Performance Polymers
2022, Vol. 0(0) 1–12

DOI: 10.1177/09540083211064972
journals.sagepub.com/home/hip

High performance based on quinoxalin-thiophene conjugated polymer composite carbon powder electrode material for Li-organic battery

Xin Yue[1], Jinsheng Zhao[2] and Lingqian Kong[1]

Abstract

In this work, thiophene derivatives were selected as donor units and pyrazine derivatives as receptor units to synthesize two composite materials consisting of supercapacitor carbon (SC) loaded with poly [2,3-bis (2-pyridinyl)-5,8-bis (2-thiophenyl) quinoxaline] (PPTQ) or poly [2,3-bis (2-pyridinyl)-5,8-bis (2-(3,4-ethylenedioxythiophene) quinoxaline] (PPETQ) by cationic radical polymerization. First, chemical bonds structure, surface morphology, and element valence states of these materials were characterized by infrared (IR), scanning electron microscopy (SEM) and XPS in turn. CV curves were used to determine their initial oxygen reduction potentials and to calculate their HOMO and LUMO values, both polymers have a narrow band gap, with E_g values lower than 2 eV. The polymer composite materials were tested as anodes in lithium-ion batteries, with a lithium sheet used as the counter electrode. Then the constant current charge-discharge and electrochemical impedance spectroscopy (EIS) impedance were measured. The first discharge specific capacities of PPTQ@SC and PPETQ@SC were 895.9 mAh/g and 913.0 mAh/g at a current density of 100 mA/g, the formation of a SEI film occurred in the second cycle, and their coulomb efficiencies can reach more than 90% from the third cycle, and the discharge platform appeared at about 1.0 V. In contrast, due to its stronger electron-donating ability, the PPETQ polymer containing the 3,4-ethylenedioxythiophene (EDOT) group have better electrical conductivity and its honeycomb structure provides more active sites for the lithiation/delithiation redox process. Therefore, the specific capacity of PPETQ@SC are all higher than that of PPTQ@SC at different current densities.

Keywords

pyridine unit, thiophene derivatives, supercapacitor carbon, donor-acceptor composites

Introduction

Lithium-ion batteries are green energy storage devices with great development potential. Only just a few decades, they have rapidly replaced other types of batteries in the market and are widely used in electronic products and electric vehicles.[1,2] In recent years, the mature inorganic[3,4] materials have been widely used in commercial lithium-ion batteries, but these materials have inherent shortcomings such as low theoretical specific capacity and stable structure that are difficult to improve.[5,6] At present, organic polymer electrode materials[7] with large theoretical capacities and flexible and designable structures have attracted an increasing amount of attention, many researchers have designed and prepared various conductive polymers[8–12] with good properties. To further enhance the electrochemical performance of lithium-ion batteries, the combination of conductive polymers and carbon materials[13,14] can be applied to form composite electrode materials. These materials can avoid the decomposition of active substances in the electrolyte and provide an excellent conductive network for the polymer.

Pyrazin-based polymers[15,16] have a strong electron deficient ability that can reduce their HOMO energy level, improving the electrochemical characteristics. Therefore, they are widely used as electron receptor units for the construction of efficient polymer electrode active materials.

[1]College of DongChang, Liaocheng University, Liaocheng, China
[2]School of Chemistry and Chemical Engineering, Liaocheng University, Liaocheng, China

Corresponding authors:
Jinsheng Zhao, College of DongChang, Liaocheng University, Liaocheng, China.
Email: j.s.zhoa@163.com

Liaocheng Kong, College of DongChang, Liaocheng University, Liaocheng, China.
Email: konglingqian@126.com

Thiophene and its derivatives, as excellent electron donor units,[17,18] are widely used in the synthesis of various organic semiconductor materials. In this work, we combine receptor and donor units to build two new conjugated polymers with low band gaps, and the composites between the polymers and carbon are formed through the in situ polymerization of the polymers on the supercapacitor carbon powder. This strategy improves the specific capacity and cycle stability of lithium-ion batteries. Moreover, the alternating distribution of donor and acceptor units along the backbone chain of the polymer enhances the π electron delocalization[19] and facilitates the storage of lithium ions.

Herein, two narrow-band-gap alternating conjugated polymers were synthesized by a coupling reaction with thiophene derivatives as donor units and pyrazine derivatives as receptor units: poly [2,3-bis (2-pyridinyl)-5,8-bis (2-thiophenyl) quinoxaline] (PPTQ) and poly [2,3-bis (2-pyridinyl)-5,8-bis (2-(3,4-ethylenedioxythiophene) quinoxaline] (PPETQ). This work is expected to provide inspiration and assistance for the rational design of lithium-ion battery materials through an investigation of the relationship between the chemical structure and electrochemical properties of the synthesized polymer materials.

Experimental

A pyridine group is introduced into the pyrazine unit of quinoxaline[20] to increase the electron-attracting ability of the receptor unit and the lithium storage performance of the polymer. The synthesis of composite materials is mainly divided into three steps, including the synthesis of 2,3-double pyridine-5,8-dibromoquinoxaline, the synthesis of monomers PTQ and PETQ, and the synthesis of the composite between the polymer (PPTQ or PPETQ) with supercapacitor carbon powder (SC) in a situ manner.

Synthesis of receptor

4,7-dibromo-2,1,3-benzothiadiazole (5.75 g) and anhydrous ethanol were added to a round-bottomed flask, $NaBH_4$ (16.5 g) was added to the flask in three additions during a 48 h stirring reaction in ice water, and white solid 3,6-dibromo-1,2-phenylenediamine (PDA) (3.38 g, 65%) was obtained by filtration. 1.03 g of PDA was then mixed with 2-bipyridine (0.806 g), 6 mL of p-toluenesulfonic acid, 25 mL of ethanol in a 100 mL round bottom flask, this mixture was heated and refluxed for 3 h, after cooled down to room temperature, 1.16 g of yellow 2,3-double pyridine-5,8-dibromoquinoxaline was obtained by filtration, and the product was washed with deionized water and ethanol. The main synthesis steps for obtaining this receptor unit are shown in Scheme 1.

Synthesis of [2,3-bis (2-pyridinyl)-5,8-bis (2-thiophenyl) quinoxaline] and [2,3-bis (2-pyridinyl)-5,8-bis (2-(3,4-ethylenedioxythiophene) quinoxaline] monomers

Scheme 2 shows the cross-coupling reaction synthesis routes of the PTQ and PETQ monomers. The synthesized receptor unit as described in *Synthesis of receptor* (1.768 g) and an excess of two different tributyltin-thiophene compounds were dissolved in the tetrahydrofuran, using diphenyl phosphine palladium chloride (0.28 g) as the catalyst, the solution was refluxed under a nitrogen atmosphere for 24 h, then transferred the mixture to a rotary evaporator to obtain the corresponding raw product. Finally, the raw products were purified on a silica gel column with a mixed solvent of n-hexane and dichloromethane (2:1 v/v) to get the PTQ and PETQ monomers with yellow color for both of them.

PTQ : ^{1}H NMR ($CDCl_3$, 400 MHz, ppm): d = 8.46 (d, 2H, ArH), 8.30 (d, 2H, ArH), 8.20 (s, 2H, ArH), 7.96 (t, 2H, ArH), 7.88 (d, 2H), 7.55 (d, 2H), 7.26(t, 2ArH), 7.21 (t, 2H). ^{13}C NMR ($CDCl_3$, 101 MHz, ppm): d = 157.65, 151.39, 148.31, 143.08, 138.92, 137.36, 136.94, 131.781, 129.03, 127.85, 126.89, 124.79, 123.20 HRMS (m/z, EI^+) calcd for $C_{26}H_{16}N_4S_2$, 448.56, found 448.23.

PETQ : ^{1}H NMR ($CDCl_3$, 400 MHz, ppm): d = 8.67 (s, 2H, ArH), 8.48 (d, 2H, ArH), 8.28 (d, 2H, ArH), 7.94 (t, 2H, ArH), 6.57 (s, 2H), 4.36 (dd, 8H). ^{13}C NMR ($CDCl_3$, 101 MHz, ppm): d = 157.54, 150.31, 148.23, 141.58, 140.62, 137.15, 136.96, 129.09, 128.78, 124.97, 123.03, 113.43, 103.37, 65.15, 64.53 HRMS (m/z, EI^+) calcd for $C_{30}H_{20}N_4O_4S_2$, 564.63, found 564.56.

Synthesis of the composites between polymers and carbon powder

The composite materials, denoted PPTQ@SC and PPETQ@SC, were prepared by adding supercapacitor carbon in the electrophilic substitution polymerization process of the

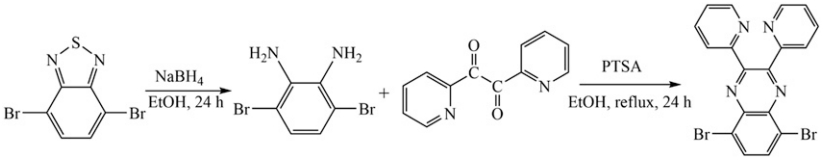

Scheme 1. The main synthetic steps of 2,3-double pyridine-5,8-dibromoquinoxaline.

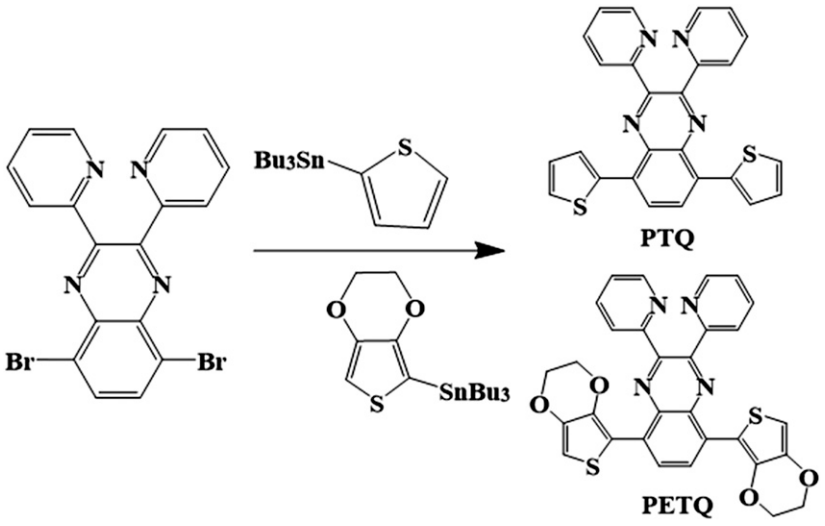

Scheme 2. The main synthesis steps of PTQ and PETQ monomers.

monomers with cationic radicals involved as shown in Scheme 3.[21] Using PPTQ@SC as an example, PTQ (100 mg), supercapacitor toner (233.33 mg) and ferric chloride catalyst (194 mg) were added to a round-bottomed flask and reacted for 48 h in 150 mL chloroform. The solid product obtained from the reaction was obtained by filtering away the solvent, and then purified in a soxhlet extraction tube with n-hexane, methanol and acetone solvents in order to remove the residual catalyst and soluble small molecule oligomers. The PPETQ@SC preparation method is the same as that of PPTQ@SC.

Material characterizations

Surface morphology were observed by scanning electron microscopy (SEM) using a JSM6380LV instrument (Japanese electronics) under 30 kV voltage, and the samples are treated with vacuum gold plating in advance. The chemical bond information of the materials was investigated using a SPECTRUM 2000 infrared (IR) spectrometer (Perkin Elmer, America) in the wave numbers range of 4000 cm^{-1} to 400 cm^{-1}. An Autosorb-1-C instrument (Quantachrome, America) was used to measure adsorption and desorption isotherms of the samples, and their specific surface areas were calculated by the Barrett-Joyner-Halenda (BJH) method. The elements and their valence states of the polymer are analyzed on an Escalab 250 photoelectron spectrometer (Thermo Scientific, America).

Electrochemical measurements

The composite powder, acetylene black and PVDF were mixed at the mass ratio of 70:20:10 with N-methylpyrrolidone as the solvent. The resulting slurry was evenly coated onto copper foil, which was vacuum dried at 90°C for 24 h and the coated copper foil was cut into 12 mm diameter electrode plates. CR2032-type cells were assembled in a high-purity Ar gas glove box (water and oxygen are below 0.1 ppm) with above prepared electrode as the anode, lithium metal as the counter electrode, polypropylene (PP, Celgard 2400) film was used as the separator, and 1M $LiPF_6$ in a mixed solvent of ethylene carbonate (EC) and dimethyl carbonate (DMC) (1:1 v/v) purchased from Merck was used as the electrolyte.

The cyclic voltammograms of the polymers were measured in tetrabutylammonium hexafluorophosphate acetonitrile solution at a scan rate of 0.1 mV/s with pseudo-Ag wire as the reference electrode. Charge and discharge curves were obtained by a LAND CT2001A battery test system (Wuhan, China) in the voltage range of 0.05–3.0 V. Electrochemical impedance spectroscopy (EIS) were carried out before and after 300 charge-discharge cycles on a Gamry electrochemical station (Reference 3000, America) with a frequency range of 0.01 Hz to 0.1 MHz and an alternating signal amplitude of 3 mV.

Characterization results and discussion

Scanning electron microscopy analysis

Figure 1 show the SEM images of the PPTQ polymer (Figure 1(a)), PPTQ@SC (Figure 1(b)), PPETQ polymer (Figure 1(c)), and PPETQ@SC (Figure 1(d)). PPTQ is composed of many disordered rod-like structures, with nanorods that are not tightly arranged and many narrow gaps in the polymer. This morphology is expected to enhance the dynamic performance of the battery to a certain extent. The surface of the PPTQ@SC material is relatively rough and some rods are

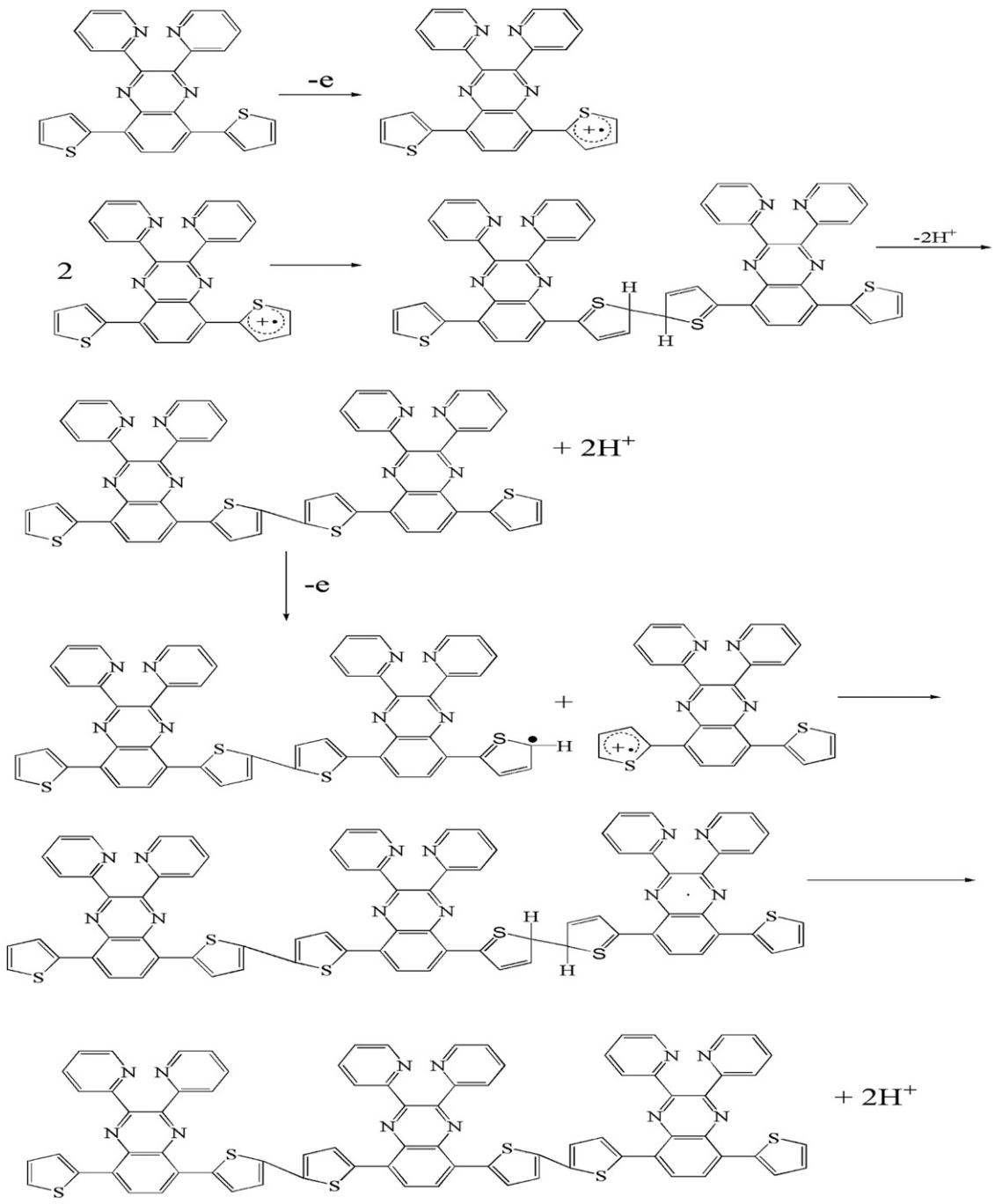

Scheme 3. The polymerization mechanism of the synthesis of PPTQ.

clearly visible on the surface, indicating that the PPTQ polymer is successfully loaded on the supercapacitor carbon through polymerization. The PPETQ polymer is shows a coral cluster structure with many nano-sized micropores. This type of pore structure can supply a better path for the diffusion and transmission of lithium ions, improving lithium-ion battery capacity. In the PPETQ@SC composite, the morphology of the PPETQ polymer changes to a honeycomb structure, and the polymer attaches to the carbon powder to form the composite successfully.

Infrared analysis

Figure 2 shows the infrared spectra of two polymer materials. Because 3,4-ethylenedioxythiophene (EDOT) has a stronger electron-donating ability than thiophene, the wave

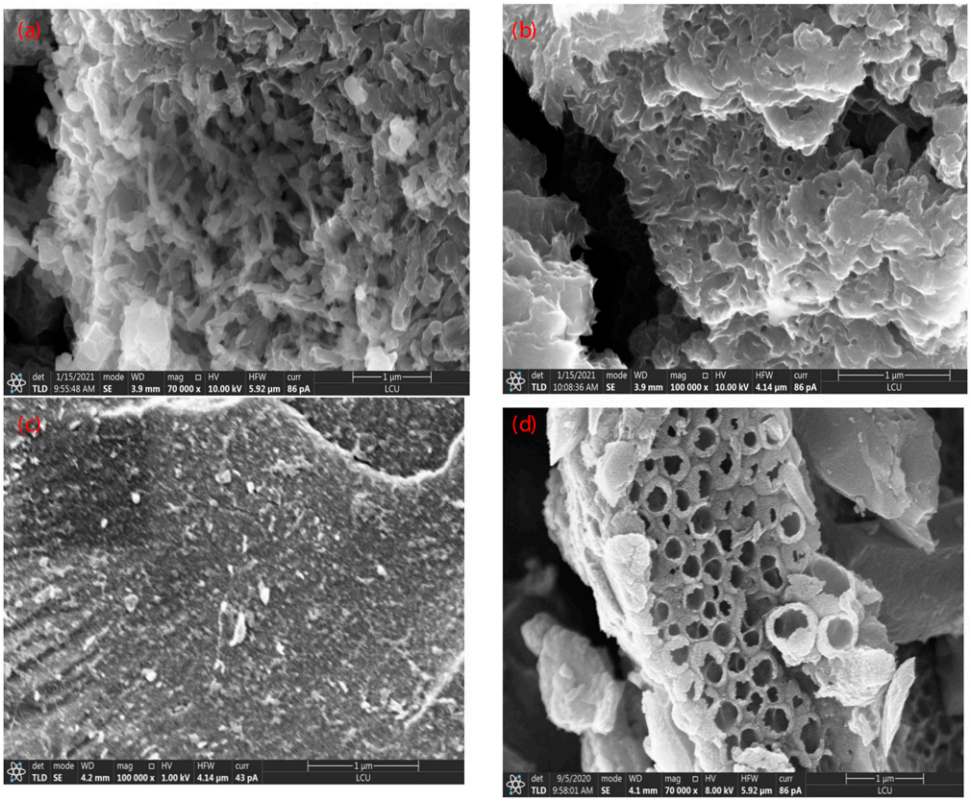

Figure 1. SEM images of PPTQ (a), PPTQ@SC (b) and PPETQ (c), PPETQ@SC (d).

numbers of the peaks of PPTQ are lower than those of PPETQ. For PPTQ, the peaks at 1508 cm^{-1}, 1396.4 cm^{-1}, and 1251 cm^{-1} correspond to the vibration of the conjugated skeleton caused by the benzene, quinoxaline, and pyridine rings, respectively. The peaks for PPTQ at 1141.5 cm^{-1} and 1041.57 cm^{-1} are ascribed to the C–H in-plane bending vibration, the peak at 795 cm^{-1} can be ascribed to the C-H out-plane bending vibration, and the peak at 1315.27 cm^{-1} can be ascribed to the C-S stretching vibration of thiophene. The skeleton vibration peaks of PPETQ appear at 1632.7 cm^{-1}, 1469.05 cm^{-1} and 1391.56 cm^{-1}, while the C-H in-plane bending vibration peak is located at 1053 cm^{-1} and the C-S and C-O vibrations of the EDOT ring are located at 1306.35 cm^{-1} and 1254 cm^{-1}.

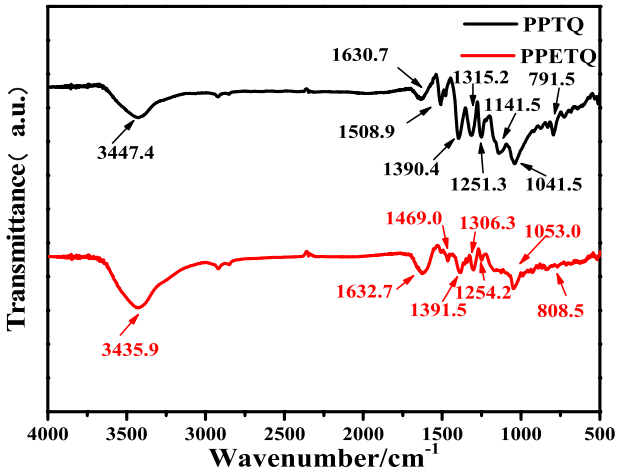

Figure 2. Infrared spectra of PPTQ and PPETQ.

Brunauer-Emmett-Teller test

Figure 3 show the nitrogen adsorption and desorption curves of PPTQ@SC (Figure 3(a)) and PPETQ@SC (Figure 3(b)). According to IUPAC classification,[22] these curves display the shape of typical IV isotherm, demonstrating that the composite materials retain the microporous structure of carbon powder. The specific surface areas of PPTQ@SC and PPETQ@SC are 584.3 m^2/g and 744.0 m^2/g by curve-fitting calculation. The higher specific surface area of PPETQ@SC is related to the existence of a higher number of nanopores in this material, and this is consistent with the presence of honeycomb structure in the composite. Higher specific surface area increases the contact area between the electrode and lithium ions during the lithiation/delithiation process, providing more active sites for the redox reaction.

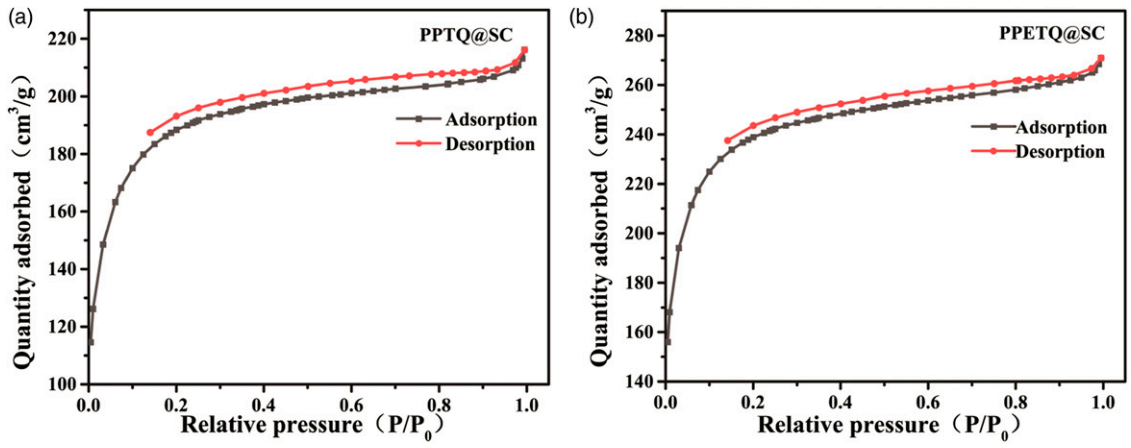

Figure 3. BET curves of PPTQ@SC (a) and PPETQ@SC (b).

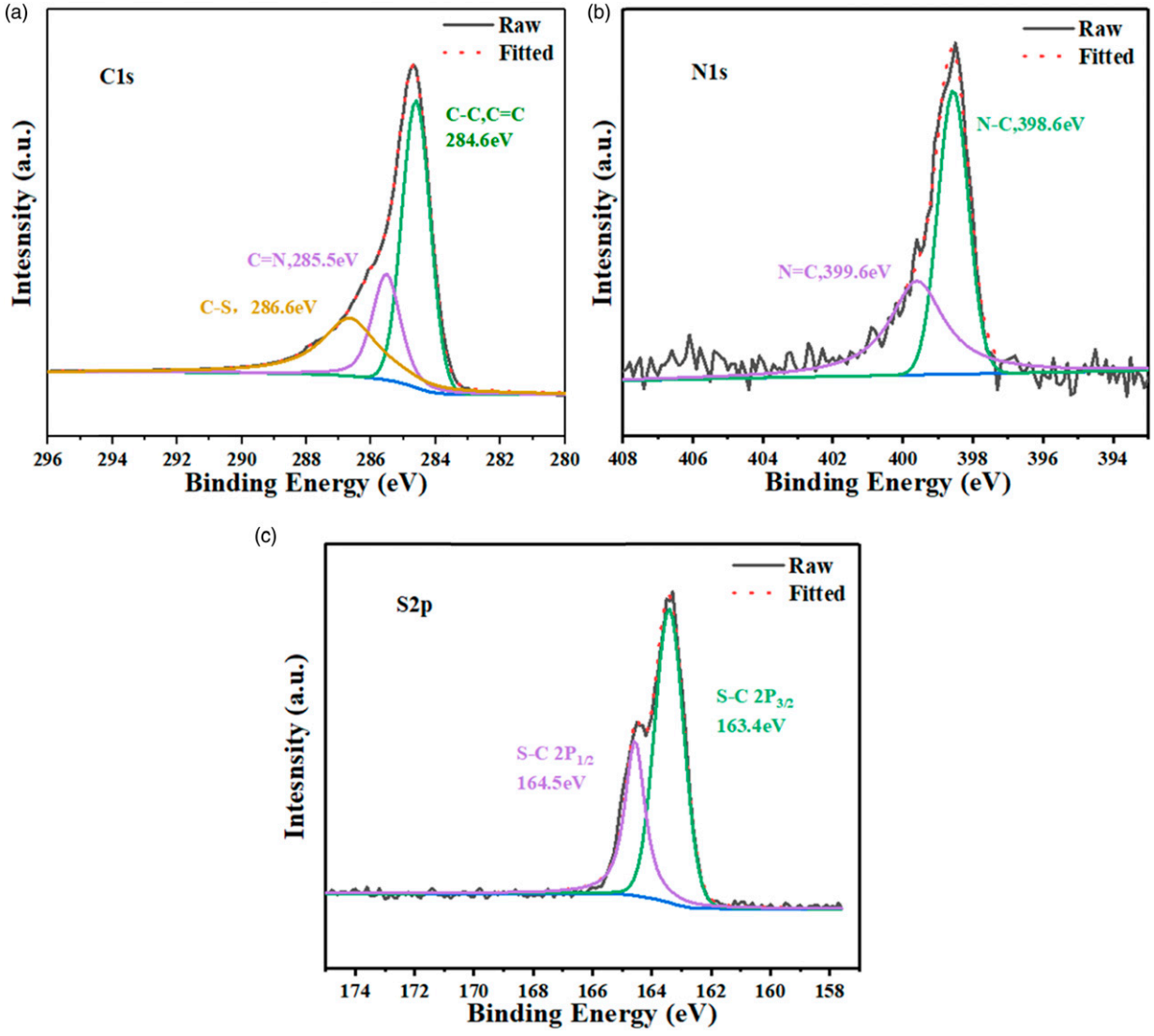

Figure 4. High-resolution XPS spectrum C1s (a), N1s (b) and S2p (c) of PPTQ@SC

X-ray photoelectron spectroscopy analysis

Figure 4 and Figure 5 show the high-resolution XPS spectra of the corresponding elements of two composites. For the C1s spectra of PPTQ composite (Figure 4(a)), the peak at 284.6 eV corresponds to the C=C in the aromatic and thiophene rings, the peak at 286.6 eV corresponds to the C-S in the thiophene ring,[23] and the peak at 285.5 eV corresponds to the C=N bond[24] of sp^2 hybridization in pyrazine. The two fitted peaks in the N1s spectra are found at 398.6 eV for N=C in pyridine ring and at 399.6 eV for the N-C in pyrazine ring,[25,26] as given in Figure 4(b). The S2p spectra for PPTQ are divided into two parts, with the peak at 163.4 eV assigned to $S2p_{3/2}$ and the peak at 164.5 eV assigned to $S2p_{1/2}$, as shown in Figure 4(c).[27] For PPETQ composite (Figure 5), because both polymers do not significantly differ in structure, the locations of C1s, N1s and S2p are similar to that of PPTQ. There is only one absorption peak in the O1s spectrum at 531.7 eV (Figure 5(d)), corresponding to the O-C bond of EDOT.[28] These results further demonstrate that the PPTQ and PPETQ composite materials were successfully prepared.

Energy level structure analysis

Pure polymer samples were coated on glass electrodes and CV curves were scanned from 2.0 V to −2.0 V in 0.2 M $TBABF_6$/ACN solution to determine the initial oxygen reduction potentials of these two polymers PPTQ and PPETQ (Figure 6). The frontier molecular orbital diagrams were obtained by using density functional theory (DFT) with the Gaussian 03 program and the B3LYP/6-31G(d) parameters, as shown in Figure 7. From the HOMO and LUMO picture we can see, there are almost no electrons in the pyridine ring, with most of the electron clouds distributed on the pyrazine unit of quinoxaline and the substituted thiophene rings, and they should be the main reactive center. In combination with the formula (1, 2, 3), we calculated the HOMO, LUMO, and E_g band gap values,[29] as listed in Table 1. Both polymers synthesized in the experiment have relatively narrow band gaps, with E_g values lower than 2 eV, and which reflect their excellent lithium storage performances. PPETQ, the polymer containing the EDOT unit, has a smaller band gap due to its better electron-donating

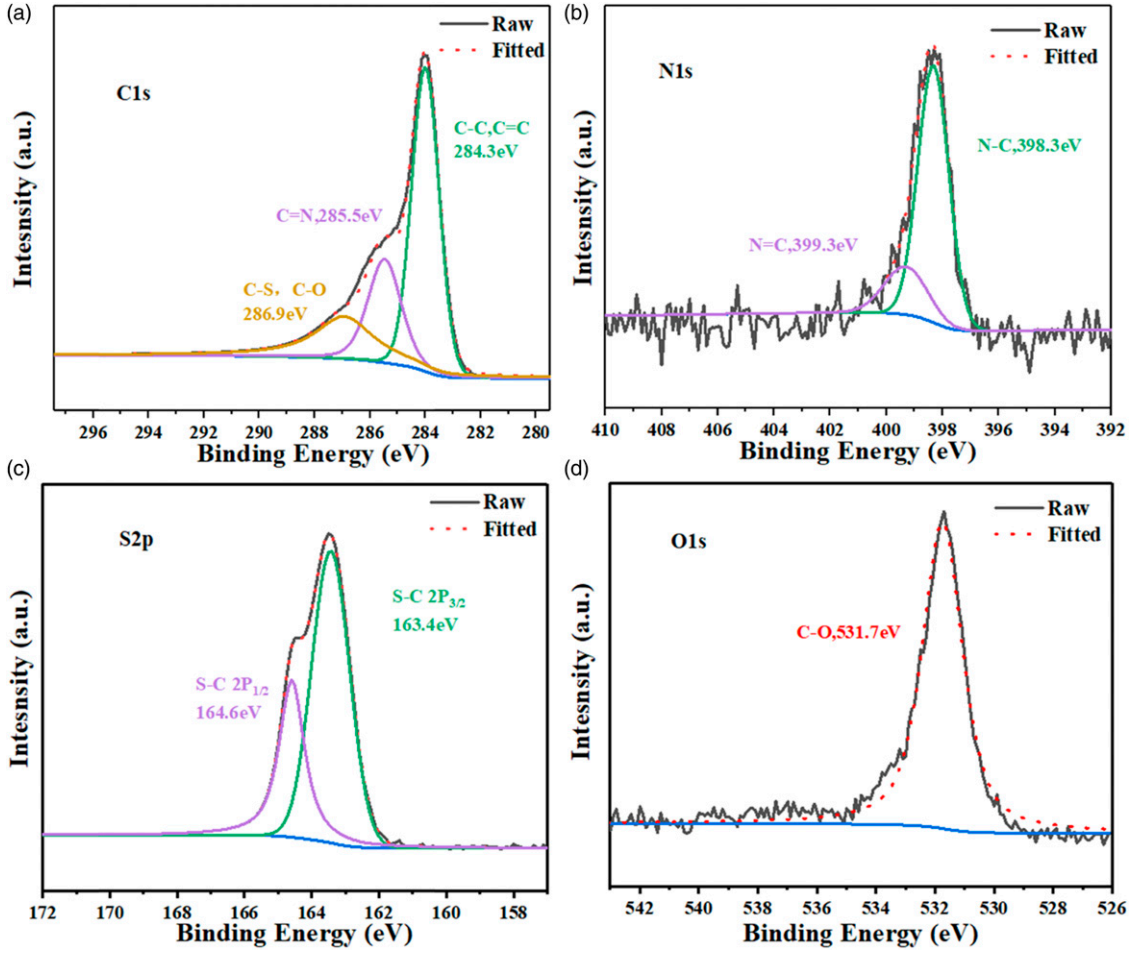

Figure 5. High-resolution XPS spectrum C1s (a), N1s (b), S2p (c) and O1s (d) of PPETQ@SC

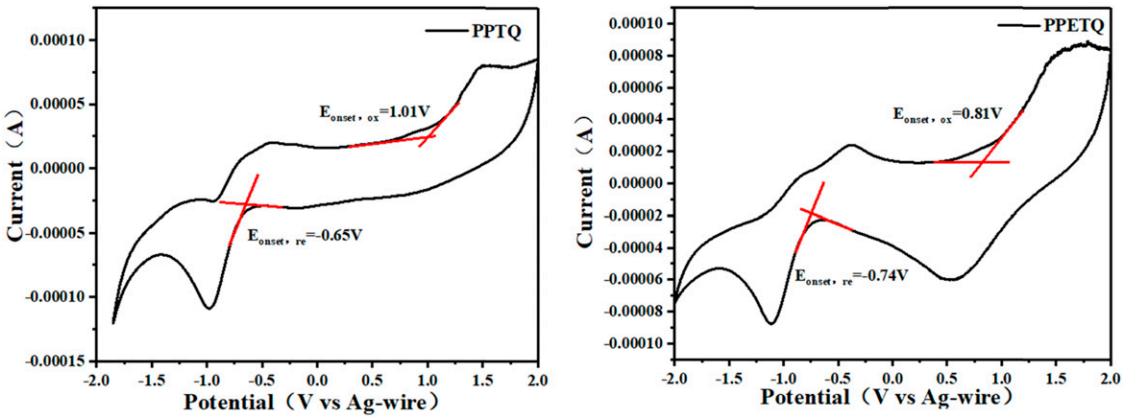

Figure 6. The CV curves of PPTQ and PPETQ electrodes at a sweep speed of0.1 mV/s.

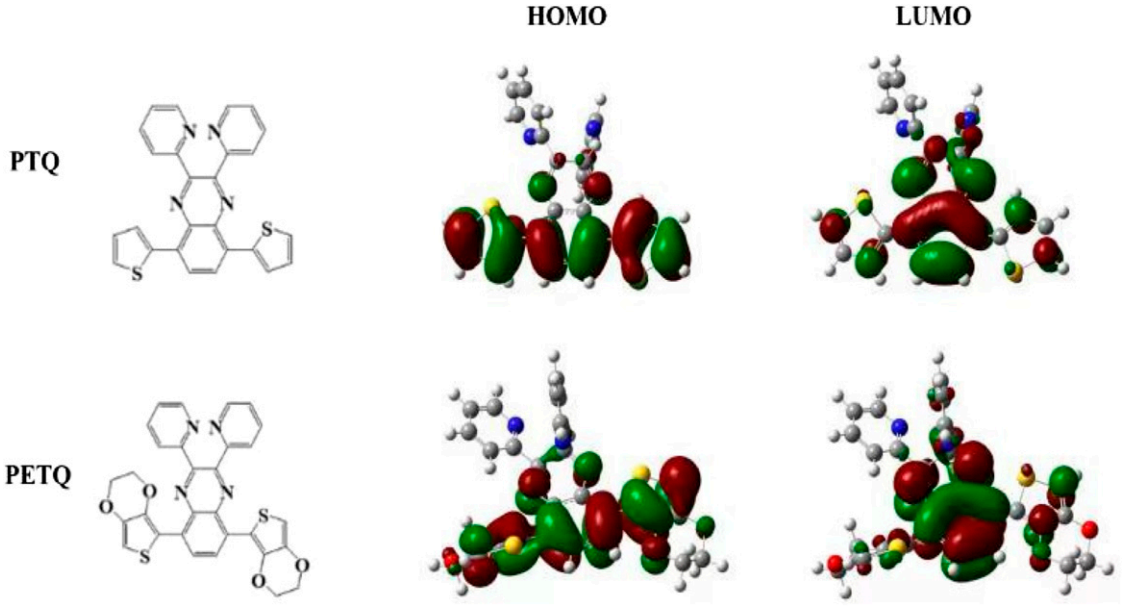

Figure 7. The molecular orbital surfaces of the HOMOs and LUMOs for two monomers.

Table 1. The parameter values of PPTQ and PPETQ.

	$E_{on,ox}$, V	$E_{on,re}$, V	E_{HOMO}, eV	E_{LUMO}, eV	E_g, eV
PPTQ	1.01	−0.65	−5.27	−3.61	1.66
PPETQ	0.81	−0.74	−5.07	−3.52	1.55

ability, resulting in higher electrical conductivity and a higher HOMO levels (−5.07 eV). Therefore, PPETQ is expected to demonstrate superior reduction properties[30] as the anode material

$$Eg = E_{LUMO} - E_{HOMO} \quad (1)$$

$$E_{HOMO} = -[4.8 + (E_{onset,ox} - 0.54)]eV \quad (2)$$

$$E_{LUMO} = -[4.8 + (E_{onset,re} - 0.54)]eV \quad (3)$$

Electrochemical performance test

Constant current charge and discharge test

Figure 8 show the lithiation/delithiation curves of the batteries using PPTQ@SC (Figure 8(a)) and PPETQ@SC (Figure 8(b)) as the anode materials at 100 mA/g, in the potential range of 0.05–3.0 V. The voltages of both composite materials experienced a rapid drop in the first turn, with the discharge platform of PPETQ composite slightly lower than that of PPTQ composite. The main discharge potential appears at about 1 V, illustrating that these new donor-receptor

type polymer anodes are conducive to be reduced, in good agreement with the low band gap of the polymers,[31,32] there are no clearly discharge platforms corresponding to the exactly functional groups in the polymer, that is also attributed to the high extended π-π conjugation backbone system. In the first cycle, PPTQ@SC and PPETQ@SC have maximum discharge specific capacities of 895.9 mAh/g and 913.0 mAh/g, respectively. In the second cycle, the specific capacity decline greatly with reversible specific capacity of 363.5 mAh/g and 402.8 mAh/g, this reveals the formation of SEI film on the surface of the composite electrode materials. In the subsequent cycles, with the disappearance of the discharge platform, the coulomb efficiency of the composite cells can reach more than 90% from the third cycle.

To study the stability of the composite materials at a high current density, the performance of the batteries was assessed over 550 cycles at a current density of 500 mA/g, as shown in Figure 9. During this lithiation and delithiation process, the specific capacities of two kinds of batteries decline first, then increase slowly, and tend to be stable gradually, which is consistent with the trend seen for the current density of 100 mA/g. With the imbedding of lithium ions into the micropores, defects and the formation of SEI film,[33,34] the capacities of the composites then go up, this might due to the enhancement in the conductivity of the composites, which make the deintercalation of lithium ions be easier, and then the electrode materials are activated. The performance of the supercapacitor carbon (SC) was also evaluated under the same conditions (the mass ratio of 70:20:10 for carbon powder, acetylene black, and PVDF), the cycling property of SC has a stable capacity of about 105 mAh/g over a long period of 550 cycles, indicating that the activation of the composites mainly occur on the polymers. At the current density of 500 mA/g, PPTQ@SC and PPETQ@SC can still maintain specific capacities of 203.7 mAh/g and 240.2 mAh/g after 550 cycles, with relatively flat charge-discharge capacities and coulomb efficiencies (CE) close to 100%. These results demonstrate that the composite materials have excellent cyclic stability, and confirm that the composite strategy based on in-situ polymerization can enhance the conductivity of the polymers and maintain the specific capacity of lithium-ion batteries. In addition, the specific capacity of PPETQ@SC is higher than that of PPTQ@SC, proving that the PPETQ with stronger electron donor group (EDOT) enhances the electrochemical performance of the resultant composite.

Ratio performance test

Figure 10 shows the ratio performance of PPTQ@SC and PPETQ@SC, with the cells charged and discharged for 10 cycles each at 100 mA/g, 300 mA/g, 500 mA/g, 700 mA/g, 1000 mA/g and 2000 mA/g, respectively, and finally go back to 100 mA/g. For both composites, the specific capacity recovers to its original level, this means that the two materials maintain a relatively stable capacity at various current amplitude, which is related to the narrow band gap and high electrical conductivity of two polymers. Besides, the reversible capacities of PPETQ@SC are significantly higher than that of PPTQ@SC under the tested current densities. The higher microporosity of the PPETQ polymer, as the binding ability of nucleus to electron is reduced, the de-intercalation process of lithium ion be easier, thus improving the kinetic parameters of the reaction.

Electrochemical impedance spectroscopy impedance analysis

Figure 11 shows the impedance diagrams of two composite batteries at an open circuit voltage (Figure 11(a)) and after 300 cycles at a current density of 100 mA/g (Figure 11(b)). Before cycling, the charge transfer resistance (R_{ct}) values of PPTQ

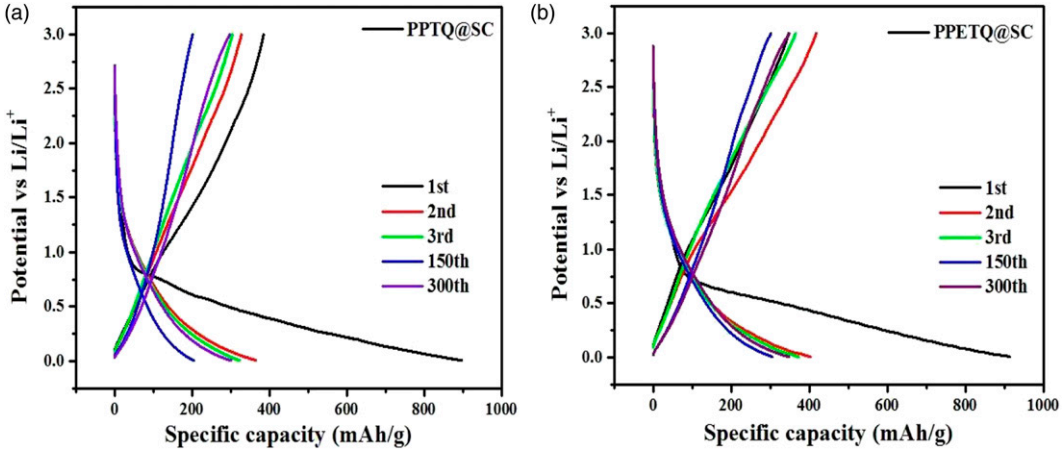

Figure 8. The lithiation/delithiation curves of PPTQ@SC and PPETQ@SC at a current density of 100 mA/g.

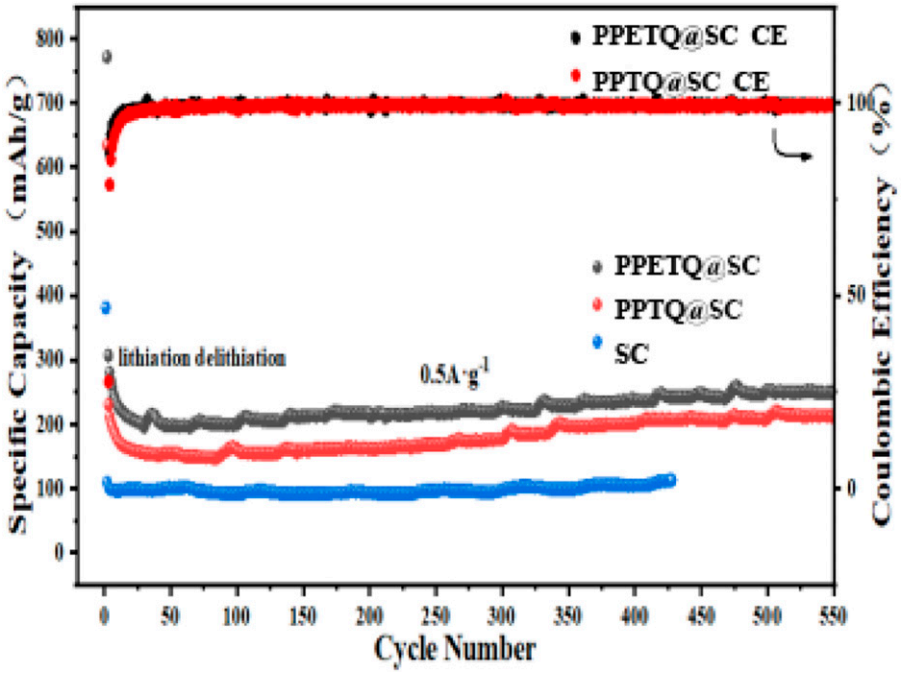

Figure 9. The lithiation-delithiation cycling performance and efficiency of two composite materials and pure supercapacitor carbon (SC) within 550 cycles at a current density of 500 mA/g.

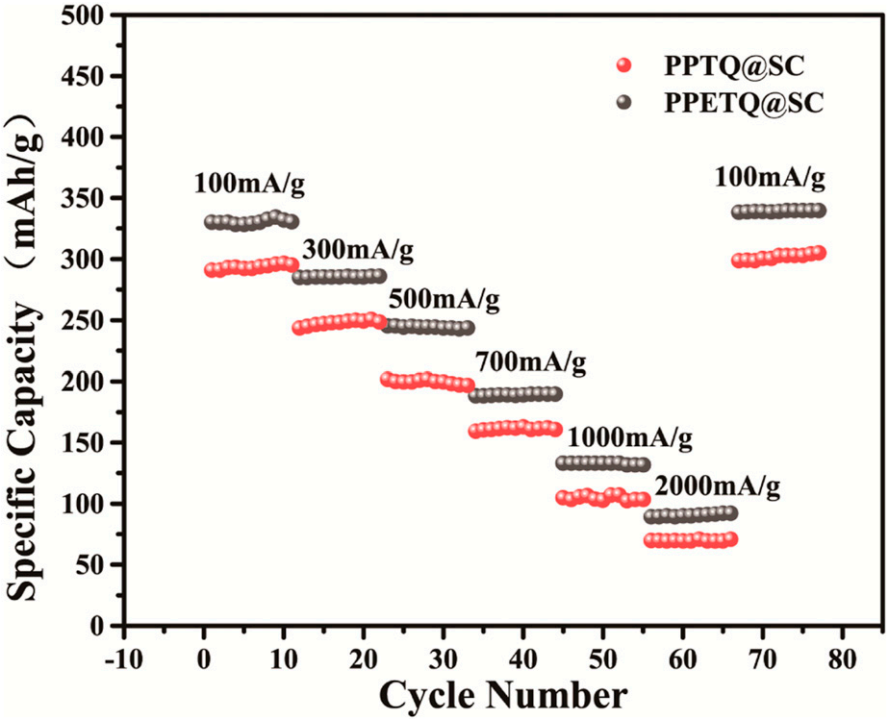

Figure 10. The cycling capacities of PPTQ@SC and PPETQ@SC at different currents.

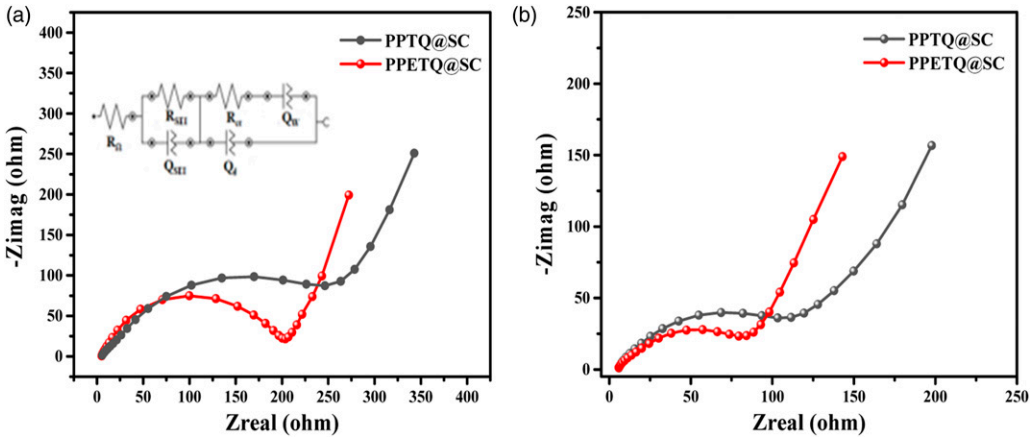

Figure 11. EIS impedance spectra of PPTQ@SC and PPETQ@SC electrodes before cycling (a) and after 300 cycles (b).

composite and PPETQ composite are 250 Ω and 202 Ω, after 300 cycles, the impedance values decline to 116 Ω and 86 Ω, respectively, showing that the electrode materials are gradually activated along with the charge-discharge reactions, this is consistent with the gradual increase in the specific capacities reported in *Constant current charge and discharge test*. In contrast, PPETQ@SC shows a lower R_{ct} value and a higher slope curve[35] than PPTQ@SC, indicating that the PPETQ polymer with a low band gap possesses superior electrochemical properties when used as an electrode material.

Conclusion

Two different composites polymer@SC were synthesized by in-situ polymerization method and were used as anode materials for lithium-ion batteries. SEM, IR, and XPS analysis confirm that PPTQ@SC and PPETQ@SC were successfully prepared. Due to the high nanoporosity of PPETQ@SC, BET test shows that it has a higher specific surface area of 744.0 m^2/g. In combination with CV curves, the E_g band gaps of PPTQ and PPETQ were 1.66 eV and 1.55 eV, respectively. With the embedding of lithium ions into the micropores and the formation of an SEI film, the specific capacities of both batteries initially decline, however, due to the enhancement of intrinsic material conductivity, which makes the disembedding of lithium ions easier, the electrode materials are activated, and their specific capacities then go up and tend to be stable gradually. At a current of 500 mA/g, PPTQ@SC and PPETQ@SC can still maintain specific capacities of 203.7 mAh/g and 240.2 mAh/g after 550 cycles. They also express good ratio stability under high current densities. In contrast, PPETQ@SC shows a lower R_{ct} value, a higher slope curve, and a narrower band gap than PPTQ@SC, indicating that the superior electron donor 3,4-ethylenedioxythiophene provides PPETQ with better electrochemical properties. Overall, these results reveal that the carbon-loaded polymer composite materials can be adjusted by changing their donor and acceptor units to achieve excellent performance in lithium-ion batteries.

Declaration of conflicting interests

The author(s) declared no potential conflicts of interest with respect to the research, authorship, and/or publication of this article.

Funding

The author(s) disclosed receipt of the following financial support for the research, authorship, and/or publication of this article: This work was supported by the Dongchang College, Liaocheng University, China (2020LG005) and Doctoral Fund Projects of Dongchang College, Liaocheng University, China (J17BS0001).

ORCID iD

Xin Yue https://orcid.org/0000-0002-2229-5060

References

1. Karden E, Ploumen S, Fricke B, et al. Energy storage devices for future hybrid electric vehicles. *J Power Sources* 2007; **168**: 2–11.
2. Li H, Wang ZX, Chen LQ, et al. Research on advanced materials for Li-ion batteries. *Adv Mater* 2009; **21**: 4593–4607.
3. Ammundsen B and Paulsen J. Novel lithium-ion cathode materials based on layered manganese oxides. *Adv Mater* 2001; **13**: 943–956.
4. Pasquier AD, Huang CC and Spitler T. Nano Li4Ti5O12-LiMn2O4 batteries with high power capability and improved cycle-life. *J Power Sources* 2009; **186**: 508–514.
5. Potapenko AV and Kirillov SA. Lithium manganese spinel materials for high-rate electrochemical applications. *J Energ Chem* 2014; **23**: 543–558.
6. Wu K, Du K and Hu G. Red-blood-cell-like (NH4)[Fe2(OH)(PO4)2]·2H_2O particles: fabrication and application in high-performance LiFePO4 cathode materials. *J Mater Chem* 2018; **6**: 1057–1066.
7. Liang YL, Tao ZL and Chen J. Organic electrode materials for rechargeable lithium batteries. *Adv Energy Mater* 2012; **2**: 742–769.

8. Li FS, Wu YS, Chou J, et al. A mechanically robust and highly ion-conductive polymer-blend coating for high-power and long-life lithium-ion battery anodes. *Adv Mater* 2015; **27**(1): 130–137.
9. Sengodu P and Deshmukh AD. Conducting polymers and their inorganic composites for advanced Li-ion batteries: a review. *RSC Advances* 2015; **5**: 42109–42130.
10. Holze R and Wu YP. Intrinsically conducting polymers in electrochemical energy technology: trends and progress. *Electrochimica Acta* 2014; **122**: 93–107.
11. Kim JK, Manuel J, Lee MH, et al. Towards flexible secondary lithium batteries: polypyrrole-LiFePO4 thin electrodes with polymer electrolytes. *J Mater Chem* 2012; **22**: 15045–15049.
12. An YL, Wei P, Fan MQ, et al. Dual-shell hollow polyaniline/sulfur-core/polyaniline composites improving the capacity and cycle performance of lithium-sulfur batteries. *Appl Surf Sci* 2016; **375**: 215–222.
13. Lian J, Wang XH, Zhang WX, et al. A ternary polyaniline/active carbon/lithium iron phosphate composite as cathode material for lithium ion battery. *J Nanosci Nanotechnol* 2016; **16**: 6494–6497.
14. Wu HP, Wang K, Meng YN, et al. An organic cathode material based on a polyimide/CNT nanocomposite for lithium ion batteries. *J Mater Chem* 2013; **1**: 6366.
15. Sifferlen T, Koberstein R, Cottreel E, et al. Synthesis, structure-activity relationship studies, and identification of novel 5,6,7,8-tetrahydroimidazo[1,5-a]pyrazine derivatives as dual orexin receptor antagonists. Part 1. *Bioorganic Med Chem Lett* 2013; **23**: 2212–2216.
16. Brown DG, Maier DL, Sylvester MA, et al. 2,6-Disubstituted pyrazines and related analogs as NR2B site antagonists of the NMDA receptor with anti-depressant activity. *Bioorganic Med Chem Lett* 2011; **21**: 3399–3403.
17. Shang ZY, Li ZC, Qin SC, et al. Backbone regulation of a bithiazole-based wide bandgap polymer donor by introducing thiophene bridges towards efficient polymer solar cells. *Organ Electron* 2021; **92**: 106130.
18. Pluczyk-Malek S, Nastula D, Honisz D, et al. Electrochemical studies of novel thiophene-tetrazine donor-acceptor hybrids. *Tetrahedron Letters* 2021; **68**: 152905.
19. Singh R, Choudhary RB and Kandulna R. Delocalization of π electrons and trapping action of ZnO nanoparticles in PPY matrix for hybrid solar cell application. *J Mol Struct* 2018; **1156**: 633–644.
20. Costa C, Farinhas J, Galvao AM, et al. On the effect of pattern substitution and oligo(ethylene oxide) side-chain modification on thiophene-quinoxaline copolymers and their applications in photovoltaic cells. *Organ Electron* 2020; **78**: 105612.
21. Rodriguez Núnez ES, Norambuena M, Romero Bohorquez AR, et al. Effificient synthesis and antioxidant activity of novel N-propargyl tetrahydroquinoline derivatives through the cationic Povarov reaction. *Heliyon* 2019; **5**: e02174.
22. Muttakin M, Mitra S, Thu K, et al. Theoretical framework to evaluate minimum desorption temperature for IUPAC classified adsorption isotherms. *Int J Heat Mass Transf* 2018; **122**: 795–805.
23. Pai CL, Liu CL, Chen WC, et al. Electronic structure and properties of alternating donor-acceptor conjugated copolymers: 3,4-Ethylenedioxythiophene (EDOT) copolymers and model compounds. *Polymer* 2006; **47**: 699–708.
24. Cano A, Rodríguez-Hernandez J, Shchukarev A, et al. Intercalation of pyrazine in layered copper nitroprusside: Synthesis, crystal structure and XPS study. *J. Solid State Chem* 2019; **273**: 1–10.
25. Pan FM, Stair PC and Fleisch TH. Chemisorption of pyridine and pyrrole on iron oxide surfaces studied by XPS. *Surf Sci* 1986; **177**: 1–13.
26. Cohen MR and Merrill RP. HREELS, ARUPS and XPS of pyridine on Ni(110). *Surf Sci* 1991; **245**: 1–11.
27. Borrelli DC, Barr MC, Bulovic V, et al. Bilayer heterojunction polymer solar cells using unsubstituted polythiophene via oxidative chemical vapor deposition. *Sol Energ Mater Sol Cells* 2012; **99**: 190–196.
28. Lisowska-Oleksiaka A, Nowaka AP, Wilamowskaa M, et al. Ex situ XANES, XPS and Raman studies of poly(3,4-ethylenedioxythiophene) modified by iron hexacyanoferrate. *Synth Metal* 2010; **160**: 1234–1240.
29. Zade SS and Bendikov M. From oligomers to Polymer: convergence in the HOMO-LUMO gaps of conjugated oligomers. *Organic Letters* 2006; **8**: 5243–5246.
30. Ye ZL, Xie SJ, Cao ZY, et al. High-rate aqueous zinc-organic battery achieved by lowering HOMO/LUMO of organic cathode. *Energ Storage Mater* 2021; **37**: 378–386.
31. Lu Y, Zhang Q, Li L, et al. Design strategies toward enhancing the performance of organic electrode materials in metal-ion batteries. *Chem* 2018; **4**(12): 2786–2813.
32. Jung KH, Jeong GS, Go CY, et al. Conjugacy of organic cathode materials for high-potential lithium-ion batteries: Carbonitriles versus quinones. *Energ Storage Mater* 2020; **24**: 237–246.
33. Xu JJ, Hu YY, Liu T, et al. Improvement of cycle stability for high-voltage lithium-ion batteries by in-situ growth of SEI film on cathode. *Nano Energ* 2014; **5**: 67–73.
34. Wang XS, Ding JY, Chen JT, et al. Improved Li+ diffusion enabled by SEI film in a high-energy-density hybrid magnesium-ion battery. *J Power Source* 2019; **441**: 227190.
35. Cruz-Manzo S and Greenwood P. An impedance model based on a transmission line circuit and a frequency dispersion Warburg component for the study of EIS in Li-ion batteries. *J Electro Chem* 2020; **871**: 114305.